Comments on wavefield propagation using Reverse-time and Downward continuation

John C. Bancroft

ABSTRACT

Each iteration a of Full-waveform inversion requires the migration of the difference between the real data and the new data created from an updated model. The migration process has typically used the Reverse-time algorithm, though alternative algorithms are now being used. The reflectivity estimate from a migration may use a cross-correlation with forward modelled data and will contains artifacts that have a very low frequency and bias the reflectivity. The cause of these low frequency artifacts is identified and evaluated using Reverse-time and Downward-continuation wavefield propagation of energy using a wavelet on a one dimensional model. The model contains varying velocities that produce multiples that are displayed with a two dimensional array in space and time. The wavefields are propagated using finite difference and phase-shift algorithms, with various initial and boundary conditions. The resulting cross-correlations are then processed to evaluate their potential for representing the reflectivity of the model.

INTRODUCTION

Motivation

Full-waveform inversion (FWI) is an iterative process that uses forward modelling and migration to estimate the rock properties of the subsurface. The ideal properties are the P and S velocities, along with the density. Practical applications currently estimate the impedance, which is a combination of the P velocities and density. The initial theory of FWI required the Reverse-time migration algorithm (RTM). This was assumed to be the ultimate algorithm as it was capable of migrating multiples, and dips up to ninety degrees. It was anticipated that use of the multiple energy would aid in reconstructing the best reflectivity model of the subsurface.

However, RTM only partially recreates the energy in the subsurface volume (x, y, z) as the required energy is not accessible from a surface recording. Consequently, only a partial reconstruction is available. In addition, the missing energy allows the reverse-time energy to produce additional unwanted energy that appears as artifacts in the reconstructed reflectivity.

Method

The flaws of RTM are demonstrated with a simple model that illustrates the effects of using data recorded on the surface to reconstruct the subsurface wavefield. A one dimensional (1D) model with varying velocities was used to forward model the primary and multiple energy as a function of space and time. The energy at all the boundaries was used with a reverse time process to reconstruct the complete wavefield with negligible error, validating the simple features of the process. Reconstruction of the wavefield using only the surface boundary was then compared with alternate methods

such as downward continuation. The Claerbout imaging condition was used to reconstruct an estimate of the reflectivity. However, the error contained in the estimated reflectivity reveals the weakness of the process.

Comments on RTM

RTM and other algorithms using the Claerbout imaging condition are really an inversion approximation, not a migration, as they attempt to estimate the reflectivity. A better name would be reverse-time inversion or RTI.

It was an objective of FWI to use all the information possible, including multiple energy, to reconstruct the reflectivity. That may not be the case now, as the FWI process assumes the input data from forward modelling and migration to contain information regarding multiples. If the modelled data was created with multiples, then the processing of the data leading to the migration should not attenuate the multiples. In contrast, if the processing sequence of the data leading to the migration has attenuated the multiples, then the forward modelling should not create multiples.

Low frequency problem

An additional problem with Reverse-time migration is the contamination with very low frequency energy. This is illustrated in Figure 1, which shows data from a Marmousi model immediately after RTM, and the same image filtered to remove the low frequency noise (Liu 2010). This example used a Laplacian filter to remove the noise.

Another example by Jiang (2012) also shows an example of data from the same Marmousi model in Figure 1a. In this case, the migration was high pass filtered, with results in (b). The amplitude spectrum of the filter is shown in (c). Details of the filter are available in Jiang (2012).

The low frequency problem is a result of using the cross-correlation used for the imaging condition (Claerbout 1971). This is not a problem of RTM but will result in any migration that uses cross-correlation for the imaging condition. The filters required to remove the low frequency noise also distort the wavelets that represent the reflectivity. For example the Laplacian filter, which for 1D data is usually defined with the three points [1 -2 1], does an excellent of removing local low frequency noise. This filter is also the finite difference approximation to the second derivative. An example of the low frequency noise is illustrated in Figure 3a, which shows a single trace that represents the direct output from a RTM. Part (b) shows the consequence of using a derivative filter, and (c) using the Laplacian filter. Note the difference in the shape of the wavelets.

More recent research has indicated that the original theory of FWI can be simplified to use any migration algorithm such as the Phase-shift method, or the Kirchhoff method as long as the modelling process matches the migration algorithm (Margrave 2010).
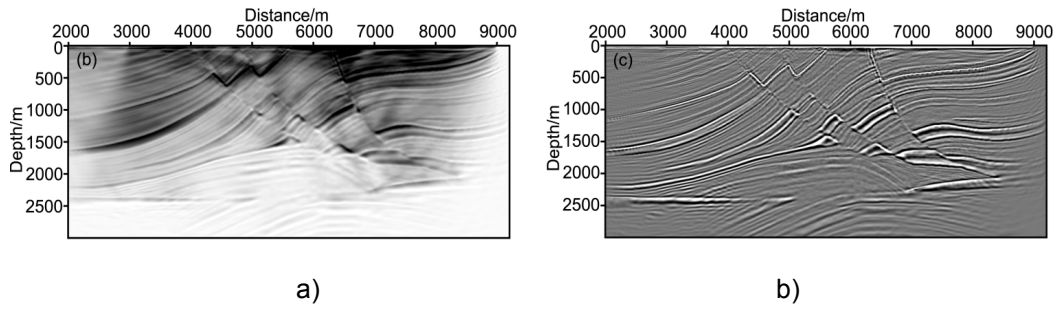
a)   b)

FIG. 1 An example of a) low frequency noise contamination, and b) after a Laplacian filter was applied (Liu 2010).

a)   b)
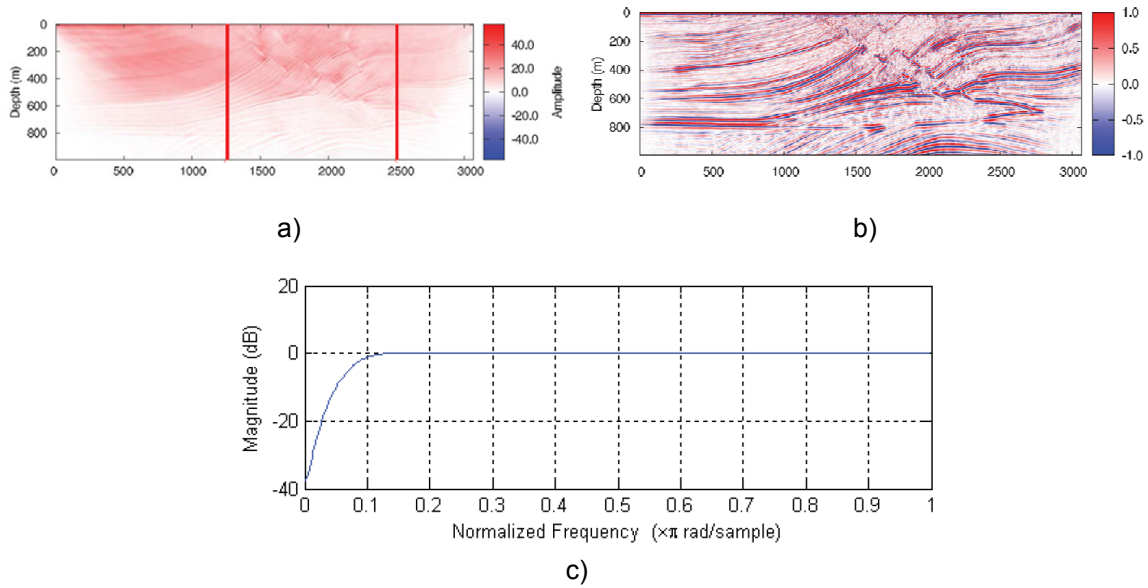

c)

FIG. 2 An example of a) low frequency noise contamination, and b) after a low pass filter was applied, and c) the amplitude spectrum of the filter (Jiang 2010).
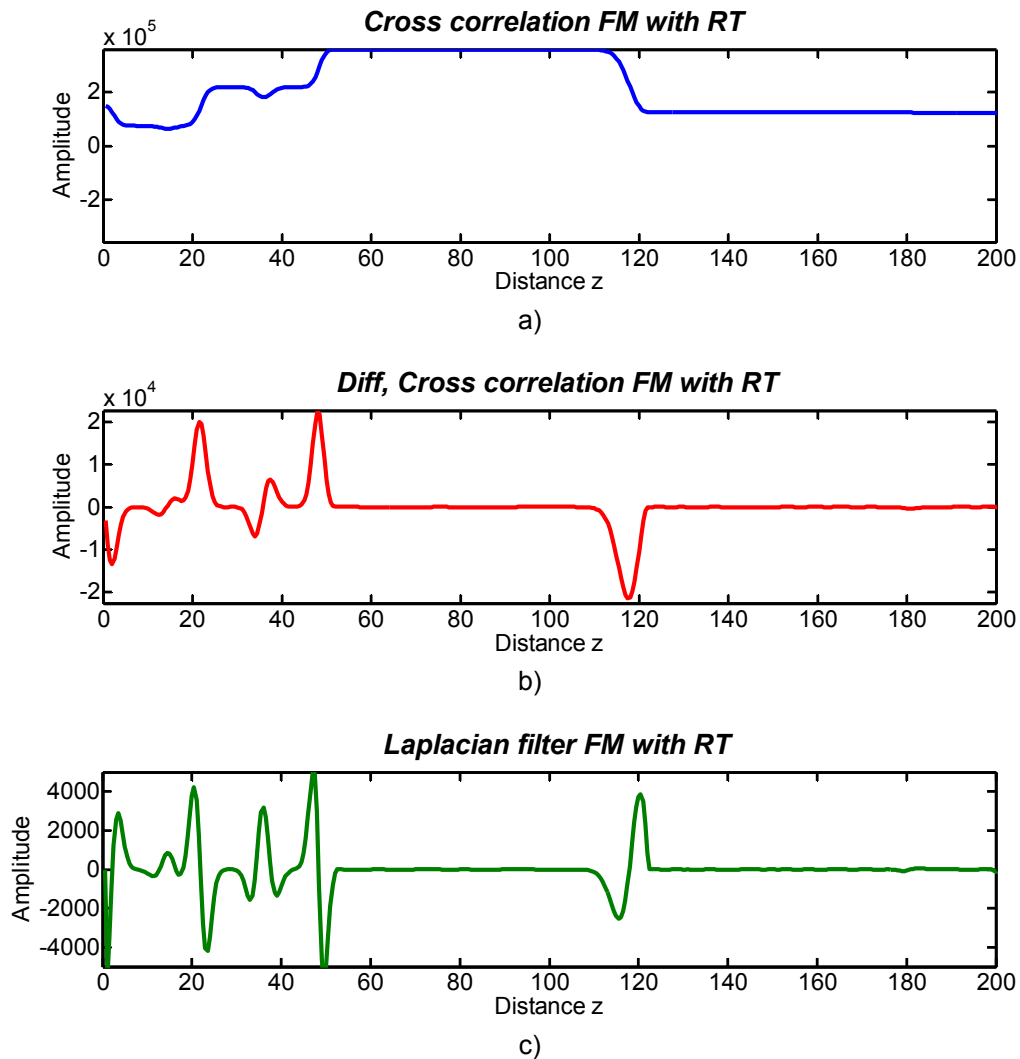
FIG. 3 Example of a cross-correlation from a RTM in a) showing the low frequency contamination, b) after a differential filter, and c) after a Laplacian filter.

THE MODELLING SYSTEM

Introduction

A simple one dimensional (1D) model was used to evaluate the wavefield. This is often referred to as the wave on a string model in which a wave propagates along a string, hits a reflecting or absorbing boundary, then propagates back along the string. This simple model has been used to demonstrate the linearity of wave propagation and the production of standing waves. The math and programing are simple, with a finite difference approximation to the wave-equation. The problem becomes more complex when the velocity of the wave on the string varies as the finite difference solution that was used assumed a constant velocity. Now the amplitudes and polarities of the reflection and transmission coefficients may be in error. I was able to circumvent many of these problems by using very high sampling rates in time and depth.

Finite difference solution to wavefield propagation

The wavefield was propagated using a two-way finite difference solution to the acoustic wave equation

$$\frac{\partial^2 P}{\partial z^2} = \frac{1}{v}\frac{\partial^2 P}{\partial t^2} , \tag{1}$$

with the second derivative approximated by (1, -2, 1) giving

$$P_{i-1,j} - 2P_{i,j} + P_{i+1,j} = \frac{\delta x^2}{v^2 \delta t^2}\left(P_{i,j-1} - 2P_{i,j} + P_{i,j+1}\right). \tag{2}$$

This solution is illustrated in Figure 4 that shows the five points and their relative location on a grid of *x* with increments in *i*, and time *t* with increments *j*.
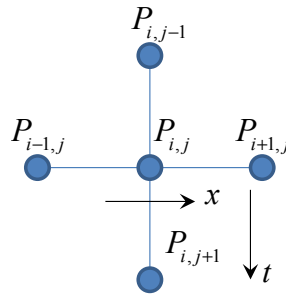
FIG. 4 Finite-difference models for the full wave equation.

The direction of propagation is controlled by solving for one of the extreme values. The movement of the energy in positive time (seismic modelling) is controlled choosing **P** at the next time location, i.e. $P_{i,j+1}$, or in reverse time (migration) as $P_{i,j-1}$. The wavefield may also be propagated in depth as in downward continuation with $P_{i+1,j}$, or in upward continuation with $P_{i-1,j}$.

For forward modelling, the finite difference solution is

$$P_{i,j+1} = 2P_{i,j} - P_{i,j-1} + \frac{v^2 \delta t^2}{\delta x^2}\left(P_{i-1,j} - 2P_{i,j} + P_{i+1,j}\right), \tag{3}$$

the reverse time solution is

$$P_{i,j-1} = 2P_{i,j} - P_{i,j+1} + \frac{v^2 \delta t^2}{\delta x^2}\left(P_{i-1,j} - 2P_{i,j} + P_{i+1,j}\right), \tag{4}$$

and the full two-way downward continuation solution is

$$P_{i+1,j} = 2P_{i,j} - P_{i-1,j} + \frac{\delta x^2}{v^2 \delta t^2}\left(P_{i,j-1} - 2P_{i,j} + P_{i,j+1}\right). \tag{5}$$

More accurate finite difference solutions are available that allow variable velocities and densities. The above simple finite difference solution is defined for a constant velocity, but in practice, it can perform reasonably well with varying velocities. In these cases, the sample intervals of δx or δt must be very small relative to the size of the wavelets. A slight error in the wavefield may occur at velocity boundaries. These errors may be undone when reversing the direction of propagation, but will become visibly evident when combining time propagations with depth propagations. The errors in location (time or space) are usually much smaller than the errors in the amplitudes.

The ratio preceding the bracketed term in equations (3) to (5) must be less than or equal to unity to ensure stability, i.e.

$$\frac{v^2 \delta t^2}{\delta x^2} \geq 1.0. \tag{6}$$

When v = 2,000 m/s, δx =0.125 m, and δt = 0.0000625 s the time modelling was stable. A time increment of δt = 0.0000626 s made the modelling unstable. Usually δx and δt are values on a grid, so the stability criterion is established with the maximum velocity.

This does create differences in the application of the algorithms when used as a time propagation or as a depth propagation as in either equations (3) and (4). The stability criterion for depth is the inverse of that for time.

$$\frac{\delta x^2}{v^2 \delta t^2} \geq 1.0. \tag{7}$$

Since the velocity of the model must be the same, a change in the grid sample intervals of δx or δt is required. I choose to increase the time sampler interval δt when propagating in depth.

Phaseshift solution

The wavefield may also be propagated with a oneway solution to the wave equation. There are numerous finite difference solutions available, but I will use the Phase-shift method for downward and upward propagation solutions. The solution in the depth-frequency domain is

$$P(z + \delta z, \omega) = P(z, \omega) e^{\pm \frac{i \delta z \omega}{v}}, \tag{8}$$

where δz is the depth increment, ω the frequency, and the sign of the exponent determines the up or down direction. This solution is ideal as the velocities are constant at each depth level, and δz can be any size over the areas with constant velocity.

The phaseshift solution is a square-root of the wave equation and requires only one initial condition at the surface, and assumes the wavefield to be moving toward $t = 0$. This is the case for all oneway solutions.

Major points of a five point FD solution

1. Efficient and simple to program.
2. Simple FD solution (grid dispersion, frequency limitation).
3. Artifacts reduced by finer sampling in x, and t.
4. Requires two initial conditions.
5. Direction of wave travel established by the second IC.
6. Requires boundary conditions at each end, (open, closed, or absorbing).
7. Forward and reverse process compensate for errors to give identical solutions.
8. Stable for propagation in one direction, e.g. t, but requires different sampling for propagation in the other direction, e.g. x.
    a. Rather than reduce the depth increment, it is easier to down sample the time data.

9. Considerable wavefield complexity can be handled with a simple model.
10. Gaussian wavelet aids in identifying polarity of the reflections.
11. Bipolar wavelet aides in verifying low frequency content in the correlations.

Boundary conditions

Each end of the string requires the definition of a boundary condition. I use three possible conditions, closed, open, and absorbing. The open and closed conditions are named after the end condition of organ pipes as illustrated in Figure 5. At a closed boundary there is no particle motion and a positive reflection results. If the organ pipe is open, then a negative reflection results. The results on a string are similar. A fixed and of the string created a positive reflection, and an end that is free to move creates a negative reflection. This is simulated by terminating the string with another piece of string with zero density. (The particle motion in the organ pipe is longitudinal, along the string it is typically illustrated as transverse.)
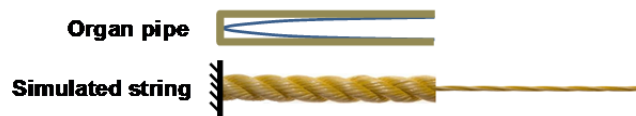

FIG. 5 Wave motion devices showing open and closed boundaries for an organ pipe and string.

My objective is to simulate wave motion within the Earth, so I choose an open boundary at the surface, and an absorbing boundary at the basement to prevent unwanted reflections.

Initial conditions

The second derivatives of the wave equation require two initial conditions. When forward modelling in time, we require two time images of the wavefield at starting times of $j = 1$ and $j = 2$, referred to as snapshots. I insert the wavelet into the string at $j = 1$, then repeat the same wavelet with an advance along the string ∇z, at $j = 2$, to define the direction that the wavelet will travel in. The distance is defined from the velocity on the string and the time increment δt, i.e., $\nabla z = V \delta t$. Note that $\nabla z \neq \delta z$.

The initial conditions and boundary values vary for the type of wave propagation that is to be considered. We traditionally think of a movie with wave motion on the string, which is defined at different times. That is forward modelling. However, we can define the initial conditions at the boundaries of the 2D data (z, t), and recreate an accurate representation of the complete wavefield.

Surface seismic assumes there is only one IC at the surface, with all other boundaries defined to be zero. We can simulate this same condition with the string model, to evaluate the effects of various initial conditions and boundary values that affect the various migration algorithms. Examples of the boundary conditions are described in Figure 6.
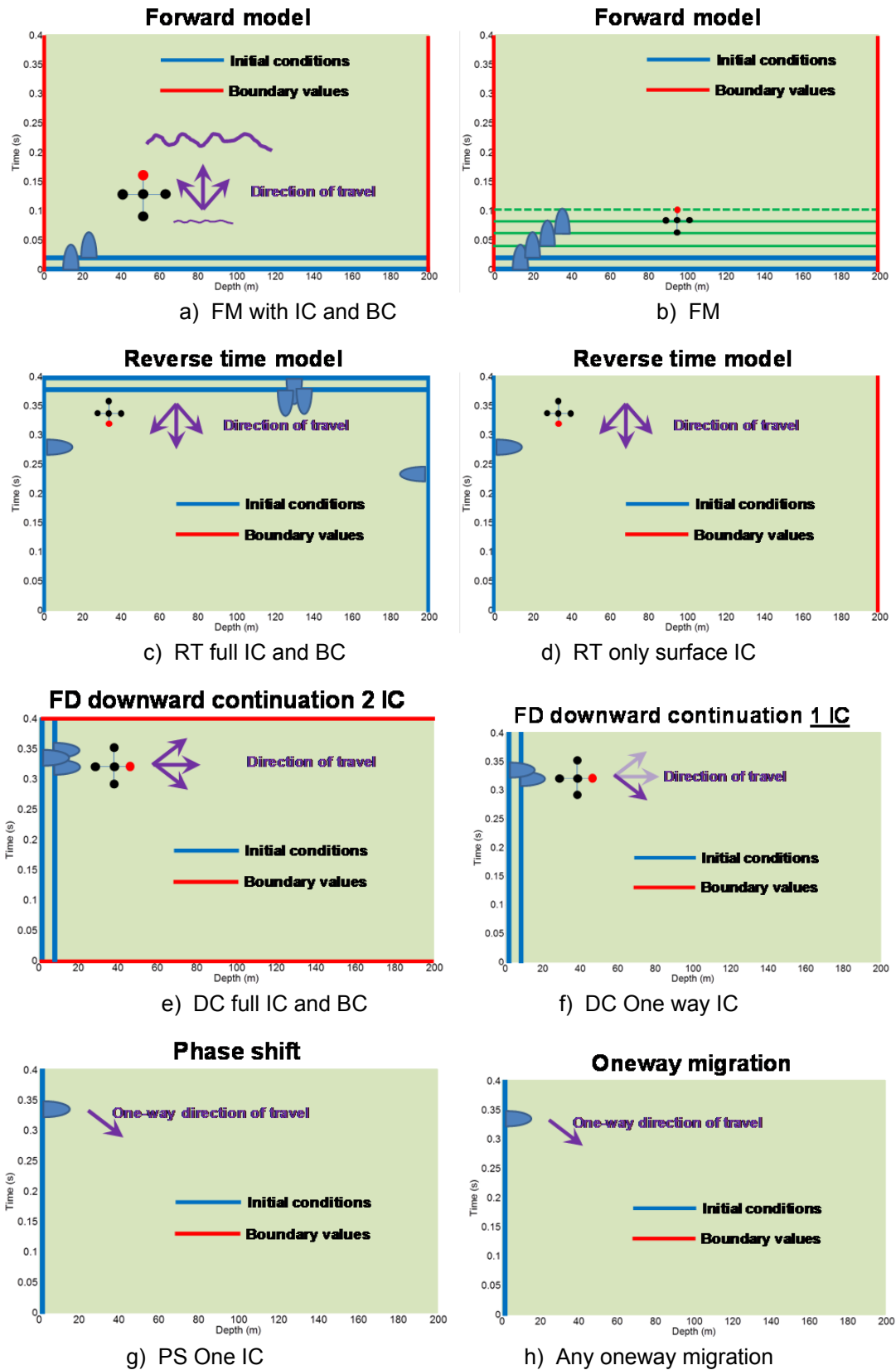
a) FM with IC and BC b) FM

c) RT full IC and BC d) RT only surface IC

e) DC full IC and BC f) DC One way IC

g) PS One IC h) Any oneway migration

FIG. 6 Initial and boundary conditions for RT and DC wave propagation.

The imaging condition and inversion

Claerbout (1971) introduced an inversion process that computed the reflectivity from an upgoing wavefield **U** that is divided by the downgoing wavefield **D**. The downgoing wavefield **D** was obtained by forward modelling the data through the subsurface using an estimate of the velocity and density, as illustrated in Figure 7a. The figure represents an expanding 2D wavefield in time (x, z, t) as it arrives at a reflecting surface, i.e. **D**, identified by the blue plane. Part (b) shows the reflected energy moving along the blue arrow towards the surface where it is recorded. I use this same figure to represent migration with the red arrow that moves the energy from the recorded data at the surface back towards the reflector using migration. At the reflector, this energy is the reflection energy **U**.

The data on the blue plane in (a) is **D** and in (b) is **U**. Rather than dividing **U** by **D**, the migration process is more stable if **D** is cross-correlated **D** with **U** to obtain an estimate of the reflectivity. This is referred to as the imaging condition where the down and up going energies are focused.

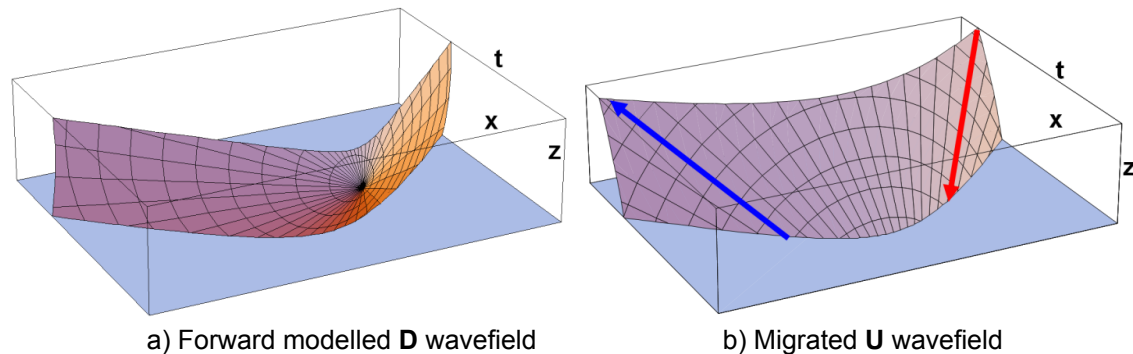a) Forward modelled **D** wavefield   b) Migrated **U** wavefield

FIG. 7 Wavefields at the imaging condition (blue plane) with a) the downward propagating wavefield from forward modelling, and b) the upward propagating wavefield (blue arrow) that has been migrated from the surface back (down) to the imaging surface (red arrow).

Computing the forward model data for the imaging condition

The data is forward modelled in time with two initial conditions at $t = 1$ and $t = 2$, a fre or open reflection at the surface $z = 0$, and an absorbing boundary at the maximum depth $z = z_{max}$. The wavefield is then create to maximum time $t = t_{max}$. This data is used as the downward propagating wavefield for cross-correlation at the imaging condition.

Computing the migrated data for the imaging condition

Since this is a modelling exercise, the forward modelled data was also used to create the simulated data that will be used for migration. Both the reverse time and downward continuation can completely recover the full wavefield when using all the data on the boundaries. That does not represent the real world case where the wavefield is only recorded as the surface, but does validate the similarities of reverse-time and downward continuation migration.

The recovered wavefield represents the upgoing wavefield **U** used for cross-correlation at the imaging condition. Cross-correlations at all depths recover an estimate of the reflectivity at all depths.

Comparisons are made of the recovered wavefield and the cross-correlation imaging condition for various initial conditions.

THE MODEL

The data in Figure 7 displayed a 2D source record in a 3D perspective view. The wavefield cannot be easily displayed as a function of time. The model chosen will be 1D seismic data, or a single trace, as if it was located at the source location *x*. This 1D model is similar to the movement of waves on a string. The amplitudes of the wavefield can then be easily displayed to show the down going incident wavelet, the primary reflection, surface multiples, and interbed multiples.

The velocities along the string were chosen to be blocky with values of 1000, 200, and 800 m/s as illustrated in Figure 8. Blocky velocities are aliased, so a smooth transition of five samples was used between each block. The maximum depth was chosen to be 200 m, with an initial sample interval of 0.25 m and the maximum time to be 0.4 s with an initial time increment of 0.00025 s. The modelling took approximately 5 seconds when using these parameters, and some error may be visible in the wavefield. These errors are not visible when sample intervals of 0.03125 m and 0.000015625 s are used.
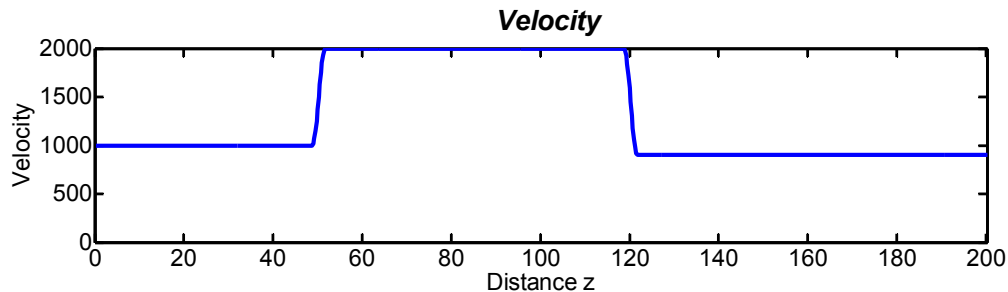

FIG. 8 Velocity array in depth.

The basement (maximum depth z_{max}) was modelled with an absorbing boundary to simulate a continuing depth model. The top surface z_0 used an open boundary to simulate the free surface where the reflection coefficient is -1. A Gaussian shaped wavelet was used as it is easy to identify its location in areas where the wavelets pass. It also has positive amplitude at zero frequency (i.e. DC component > 0). The derivative of the Gaussian wavelet is an anti-symmetric wavelet with zero amplitude at zero frequency (i.e. DC = 0). These properties were useful when evaluating the low frequencies of the reflectivity. The second derivative of the Gaussian wavelet produced a wavelet with a "W" shape that also has DC = 0.

The wavefield was initiated with wavelet energy on the first two time intervals (initial conditions) at 0.00000 and 0.00025 s as required by equation (3). These initial conditions establish the initial direction the wavelet travels, which is to the right as illustrated in Figure 9. The reflecting boundaries are indicated by blue "+" symbols. The figure also contains a wavelet (green dash) at a later time of 0.05 s to verify the preservation and

direction of travel of the wavelet after it has passed the first boundary, and also shows a reflection moving to the left. Note the change in the width and amplitude of the green wavelet when it is in the central area with high velocity.
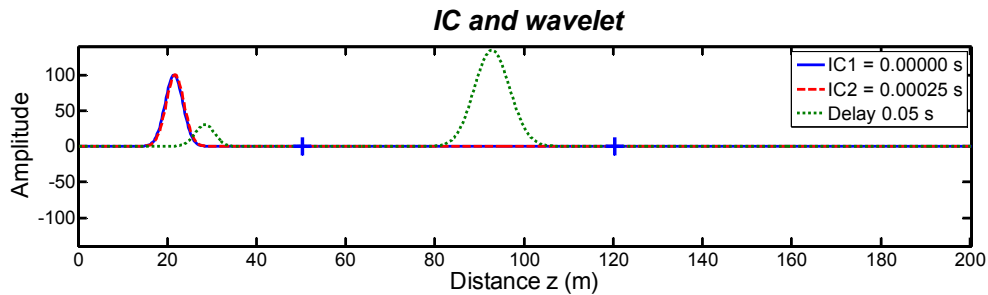

FIG. 9 Wavelets for two initial conditions, and one at time 0.010 s.

The wavefield at depths 0 and 5 m is shown in Figure 10 to illustrate the approach of the wavelets at the open boundary of the surface. At the boundary, the amplitude in blue is twice that of the body waves, represented by the green wavelets at a depth of 5 m. The body wave does contain the incident and the reflected wavelets as they spread away from their location at the surface. The wavelets arriving at approximately 0.075 and 0.15 s are primary reflections. The other wavelets are from multiple reflections.
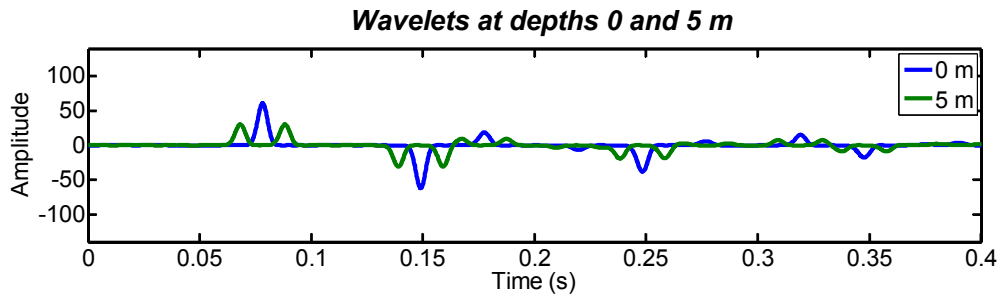
FIG. 10 Wavelets at time 0.200 and 0.210 s. The direction of movement is from the blue to the green wavelet.

The surface recording at $z = 0$ is most important as that is the data recorded with surface seismic. This is the information that we will used to recreate the energy within the subsurface using the various migration algorithms.

A three dimensional plot of the wavefield is shown in Figure 11. The downgoing incident energy, primary reflected energy, surface multiple energy, and interbed multiples can be identified. It is only the downgoing incident energy and the primary reflected energy that we desire for the cross correlation. All other energy will contribute noise.

The complete wavefield was recreated using only the energy on the boundaries, as identified by Figures 6c and 6e, using reverse time and downward continuation. The reverse time reconstruction had amplitude errors less than 10^{-12} and is not shown, however, the difference of the forward model and the reverse time reconstruction is shown in Figure 12. These small errors do not represent the accuracy of the finite difference modelling. The modelling errors that will have occurred are "undone" by using the same algorithm when reversing the wave propagation procedure.

The complete reconstruction of the finite difference downward continuation wavefield is shown in Figure 13. This process required increasing the time sample rate by 3 to maintain stability. Some differences from the forward model are identifiable but are more evident in the difference between the forward model and the reconstructed downward continuation, as shown in Figure 14.
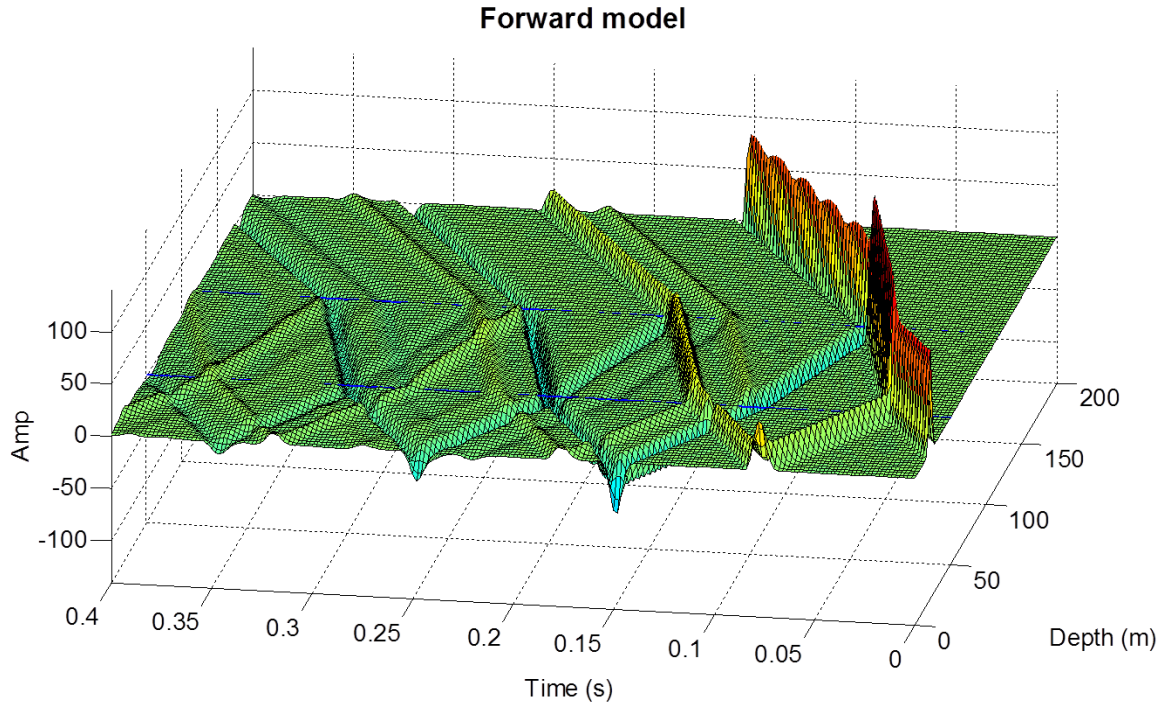
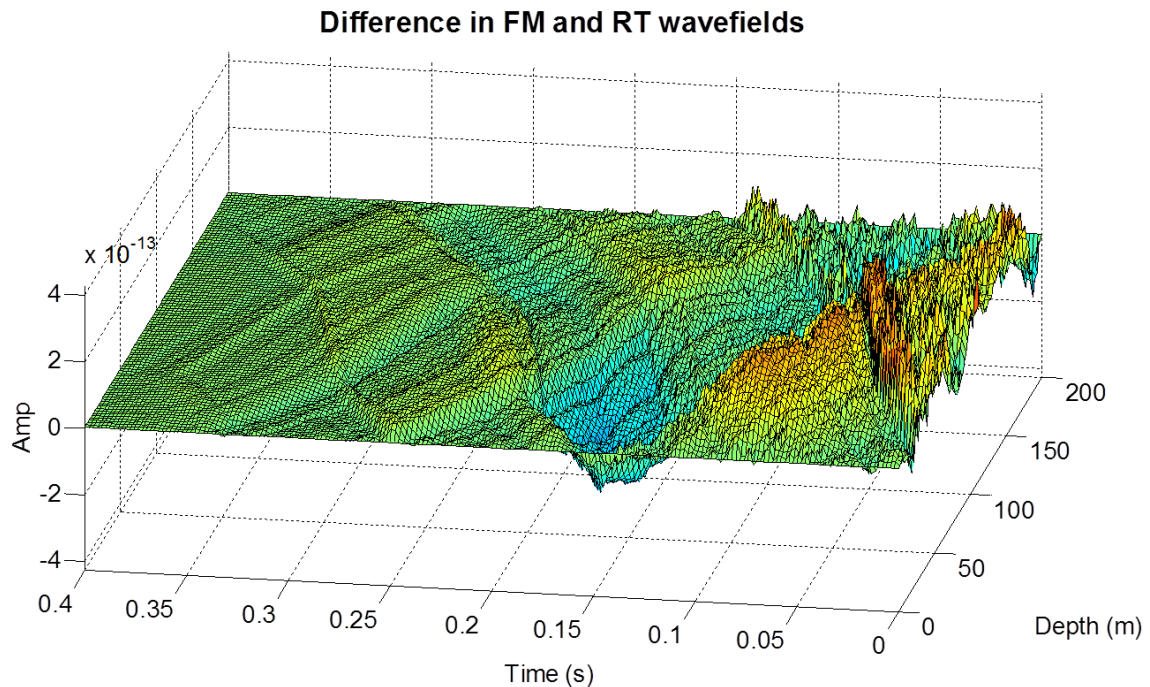**Forward model**

FIG. 11 View of the complete wavefield.

Difference in FM and RT wavefields

FIG. 12 Difference between the forward model and the reverse time reconstruction.

Downward continuation wavefield
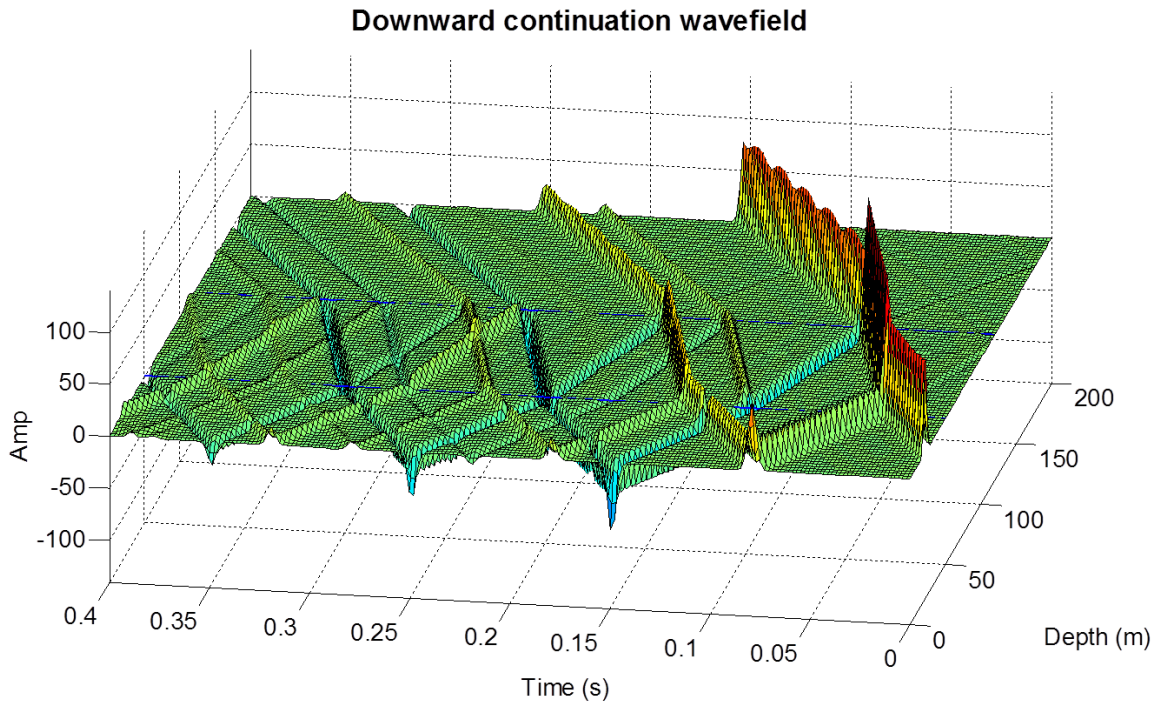
FIG. 13 Reconstructed wavefield using downward continuation.

Percent difference in FM and DC wavefields
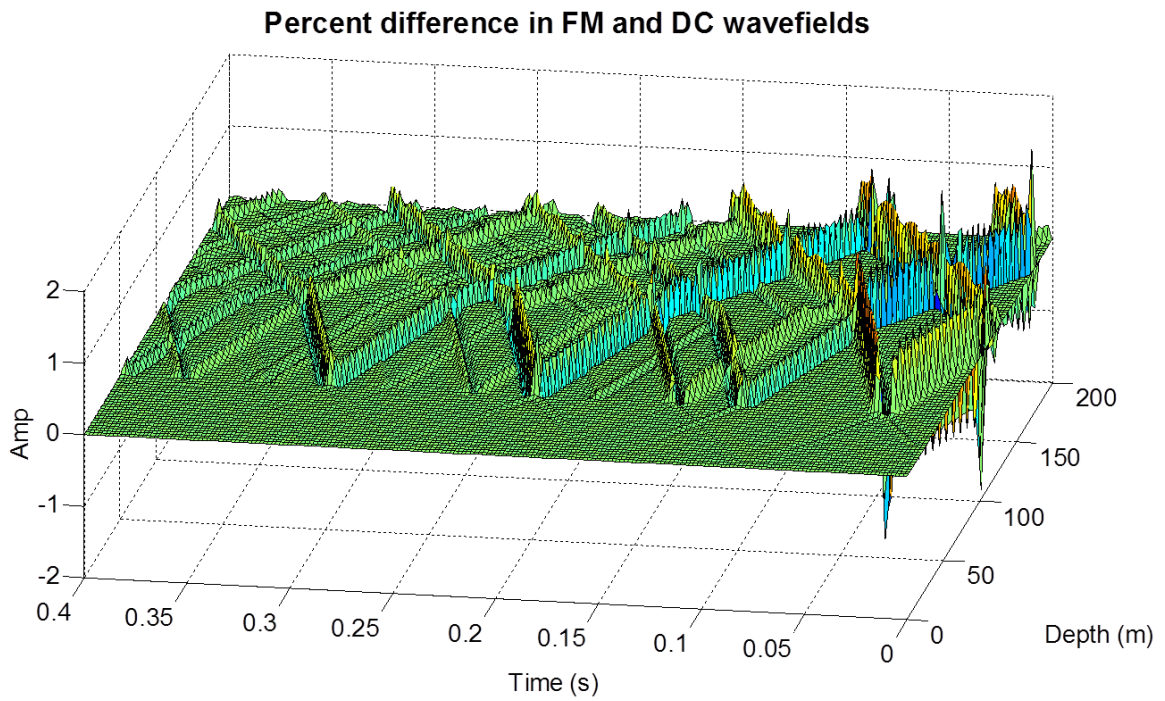
FIG. 14 Difference between the forward model and the downward continued reconstruction.

The difference between the forward model and the downward continuation reconstruction is quite large, in the order of 2%. These errors are now a result of the difference in the applications of the finite difference algorithm. This is evident by the change in error at the internal reflecting boundaries.

Wavefield reconstruction using the surface seismic.

The above wavefield reconstruction does not represent the wavefields that can be recovered using only the surface seismic. We now use only the surface seismic for the initial condition at $z = 0$. There are three examples, the reverse time in Figure 15, finite difference downward continuation in Figure 16, and the phase shift downward continuation in Figure 17. The two initial conditions for the reverse time at t_{max} are both zero. The finite difference downward continuation requires two initial conditions at the surface. This is accomplished by defining the IC at $z = \delta z$ to be the same as $z = 0$, but time shifted towards $t = 0$ with a time increment equal to the velocity multiplied by the depth increment.
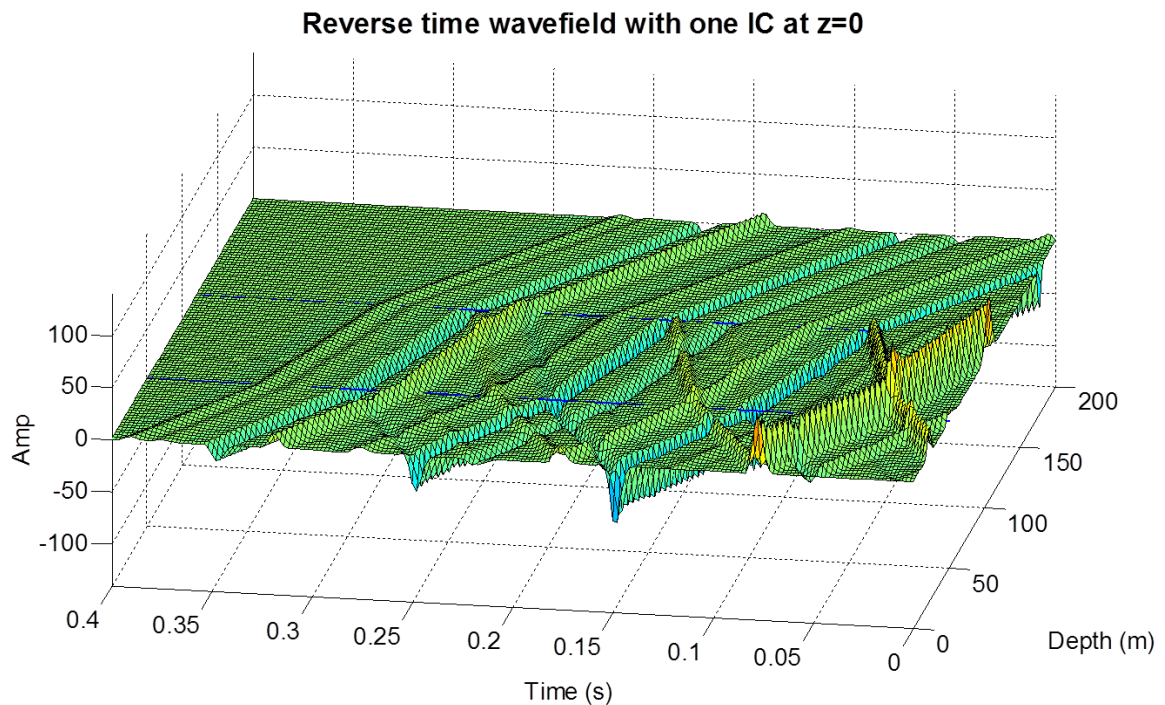

FIG. 15 Reconstructed wavefield using reverse time with only the surface IC.

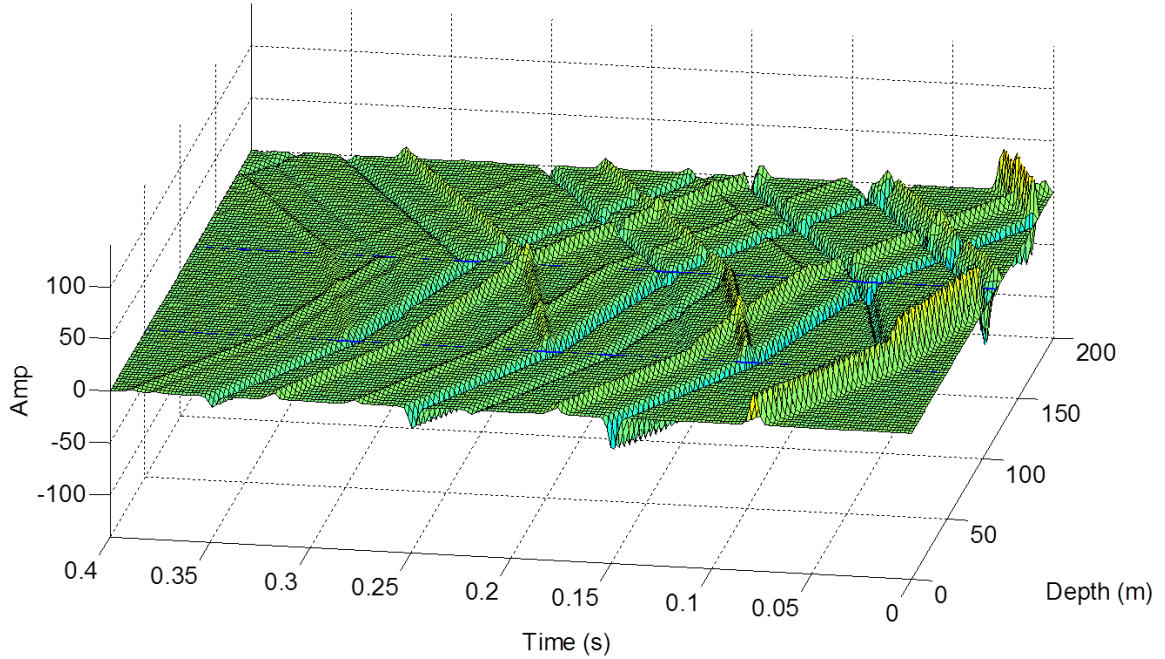**Two way DC wavefield with one IC and z = 0, second t shifted**

FIG. 16 Reconstructed wavefield using FD downward continuation with only the surface IC.
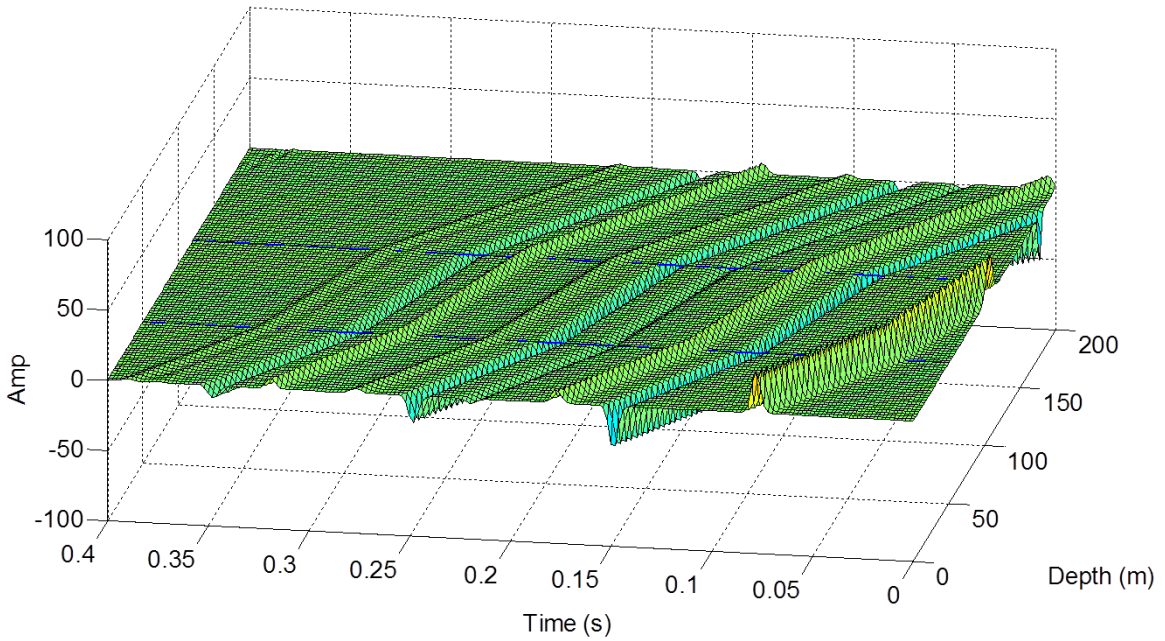
Phaseshift oneway wavefield

FIG. 17 Reconstructed wavefield using phase-shift downward continuation with only the surface IC.

Estimates of the reflectivity using cross-correlation

The reflectivity is computed from a velocity model that had smoothed transitions between the velocity interfaces. The reflectivity appears in Figure 18 as a narrow wavelet whose width is equal to the transition zone. When the velocity change is small, (not this case), the sum of the sampled reflectivity will approximate the reflectivity between the two velocity layers. However, this example is a close enough approximation to allow the peaks of the reflectivity to be close enough for visual comparisons.
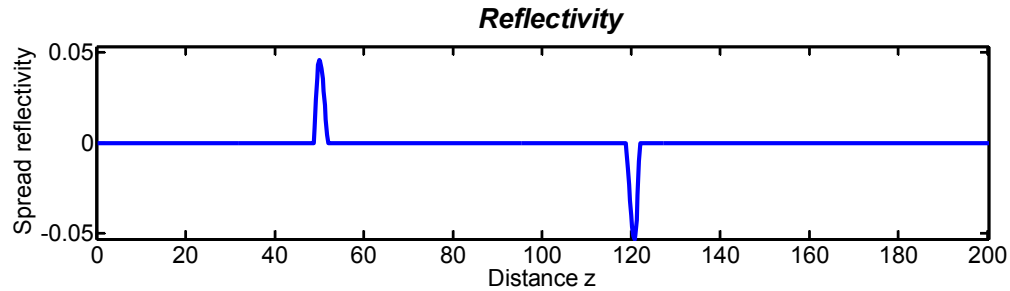

FIG. 18 An approximation to the reflectivity computed from the velocity model.

The reflectivity is estimated using the cross-correlation of the forward modelled wavefield with the reconstructed wavefields. According to the assumption of the imaging condition, we only want the initial downward propagating wave and the primary reflected waves. This is somewhat illustrated in Figure 19 where the forward and reverse time wavefield have been windowed.
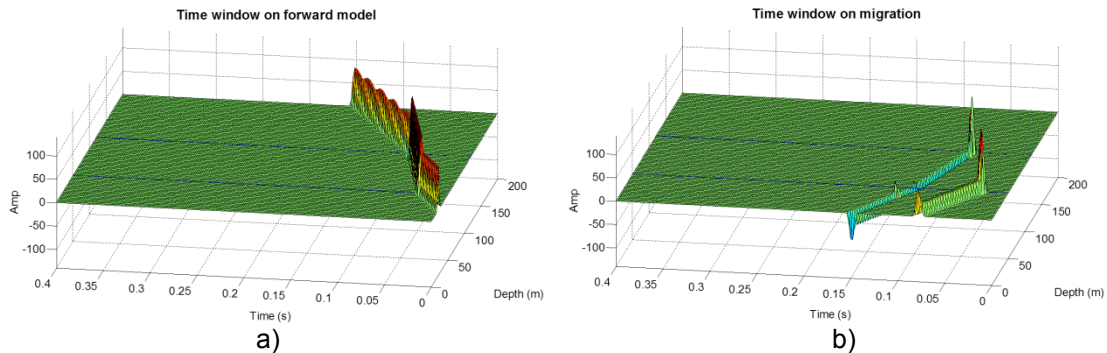

FIG. 19 The initial downgoing wave, and the primary reflected wave.

The cross correlation (CC)of the windowed forward modelled wavefield (wFM) with the windowed fully reconstructed wave filed with reverse time (wRT) is displayed in Figure 20a. The derivative of (a) is in (b) and the Laplacian filter of (a) in (c).
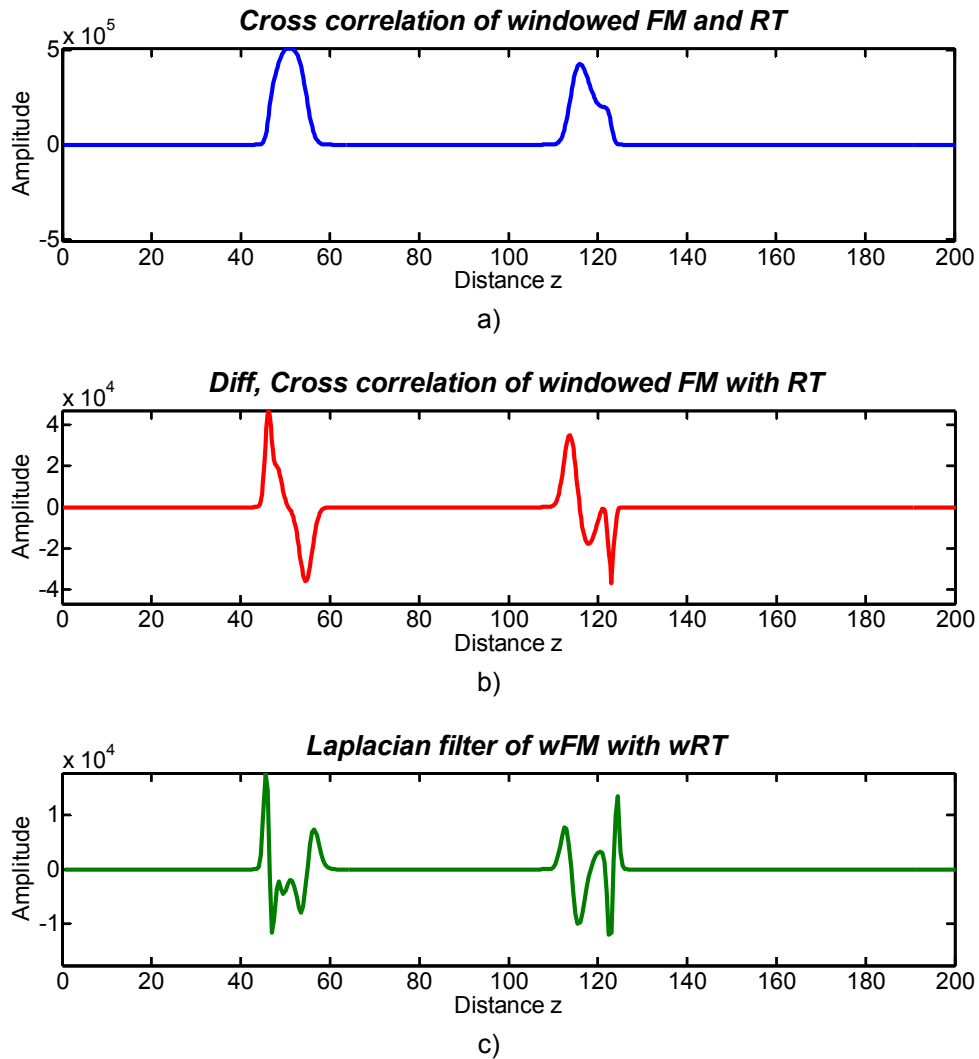

a)

b)

c)

FIG. 20 CC of wFM with wRT, a) the windowed CC, b) differentiated CC, and c) Laplacian filtered CC.

These results are supposed to be optimal, but don't even have the correct polarity.

A better result is obtained when using the windowed forward modelled (wFM) data with the complete reverse time migration (RT).
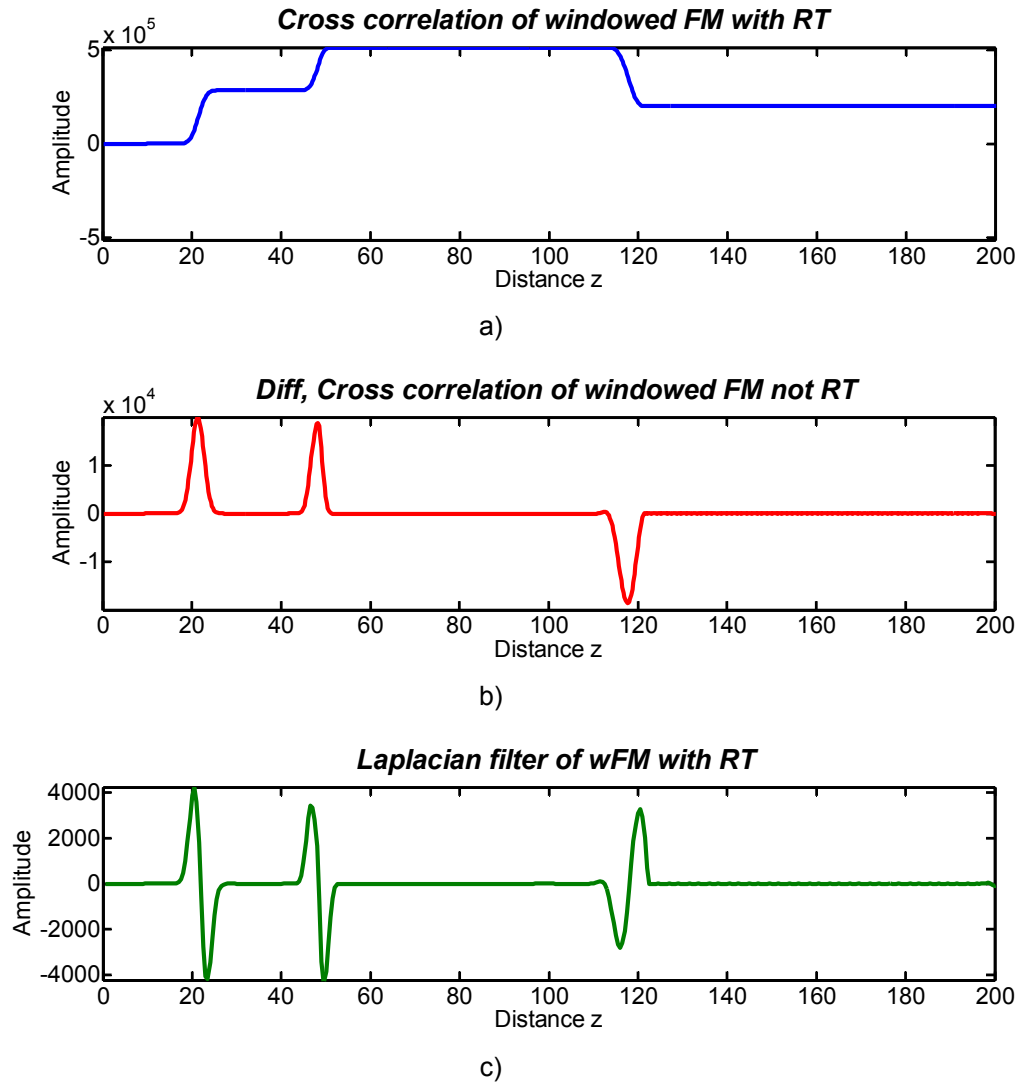

a)

b)

c)

FIG. 21 CC of wFM with the complete RT, a) the windowed CC, b) differentiated CC, and c) Laplacian filtered CC.

The CC of the fully modelled wavefield (FM) with the fully reconstructed RT wavefield is displayed in Figure 22a. The differentiated CC is in (b), and the Laplacian filtered CC is displayed in (c). (Not seismic.)

Cross correlation FM with RT

a)

Diff, Cross correlation FM with RT
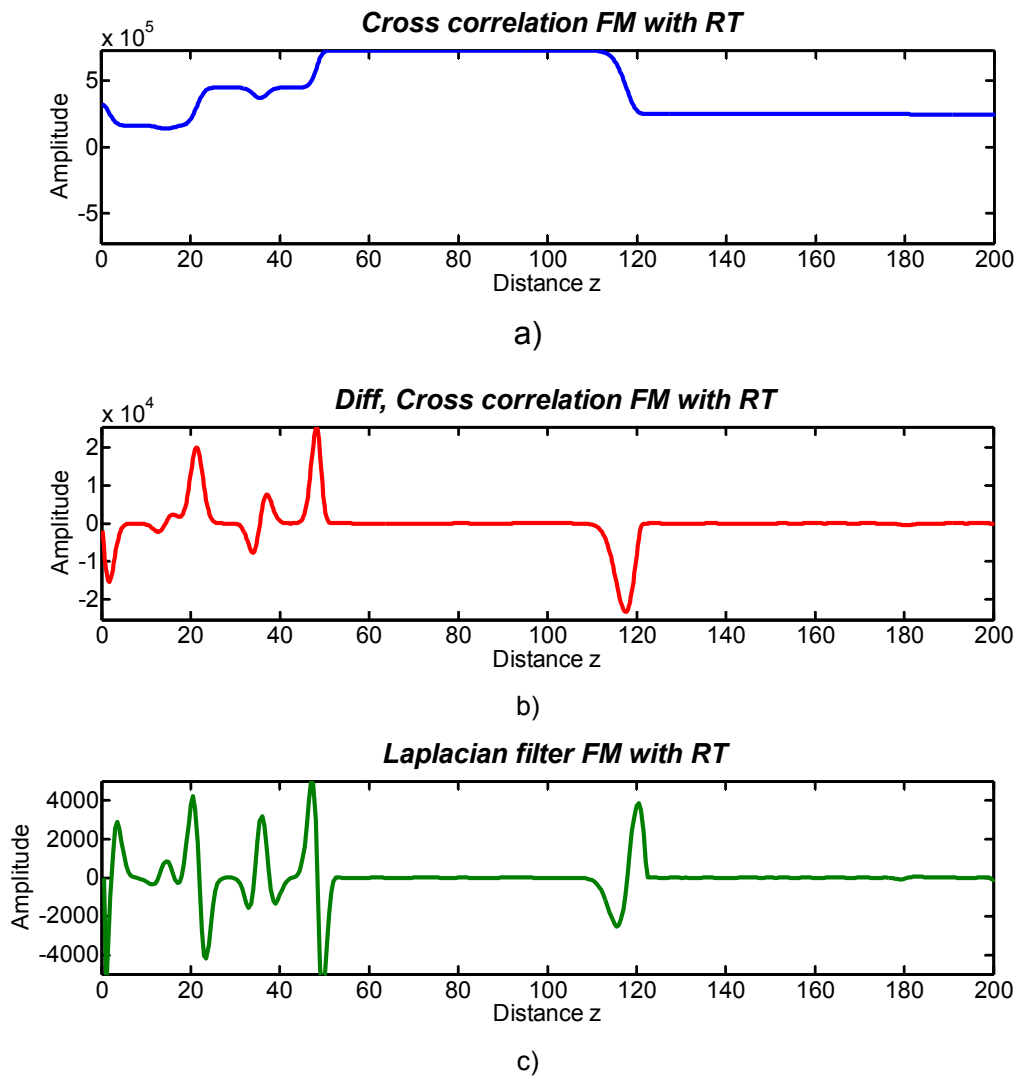

b)

Laplacian filter FM with RT

c)

FIG. 22 CC of FM with the fully reconstructed reverse time wavefield, a) the windowed CC, b) differentiated CC, and c) Laplacian filtered CC.

The CC of the fully modelled wavefield (FM) with RT using only the surface IC is displayed in Figure 23a. The differentiated CC is in (b), and the Laplacian filtered CC is displayed in (c).
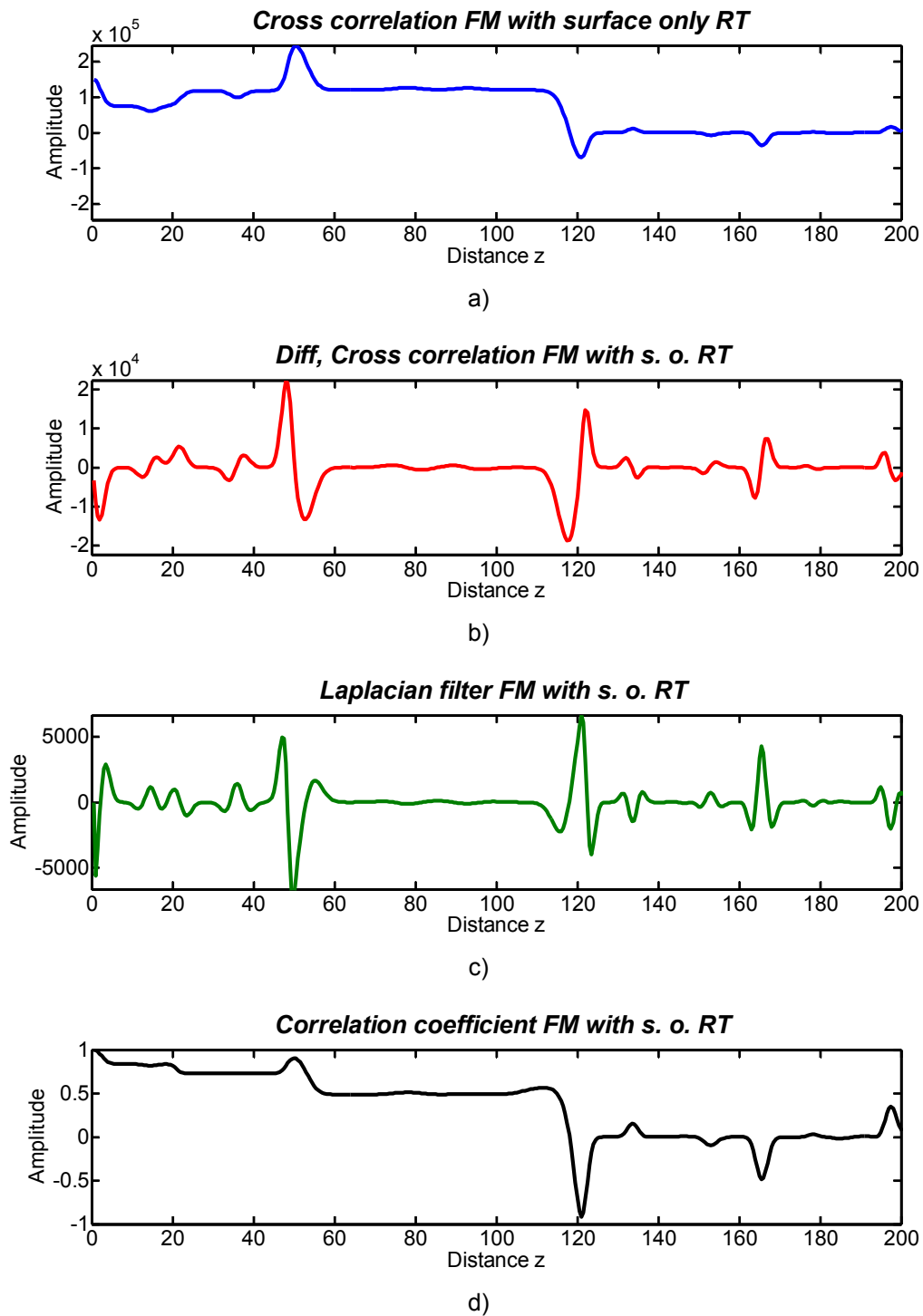

a)

b)

c)

d)

FIG. 23 CC of FM with the reconstructed reverse time wavefield using only the surface IC, a) the windowed CC, b) differentiated CC, c) Laplacian filtered CC, and d) the correlation coefficient.

The CC of the fully modelled wavefield (FM) with the migrated downward continued wavefield using only the surface IC is displayed in Figure 23a. The differentiated CC is in (b), and the Laplacian filtered CC is displayed in (c).
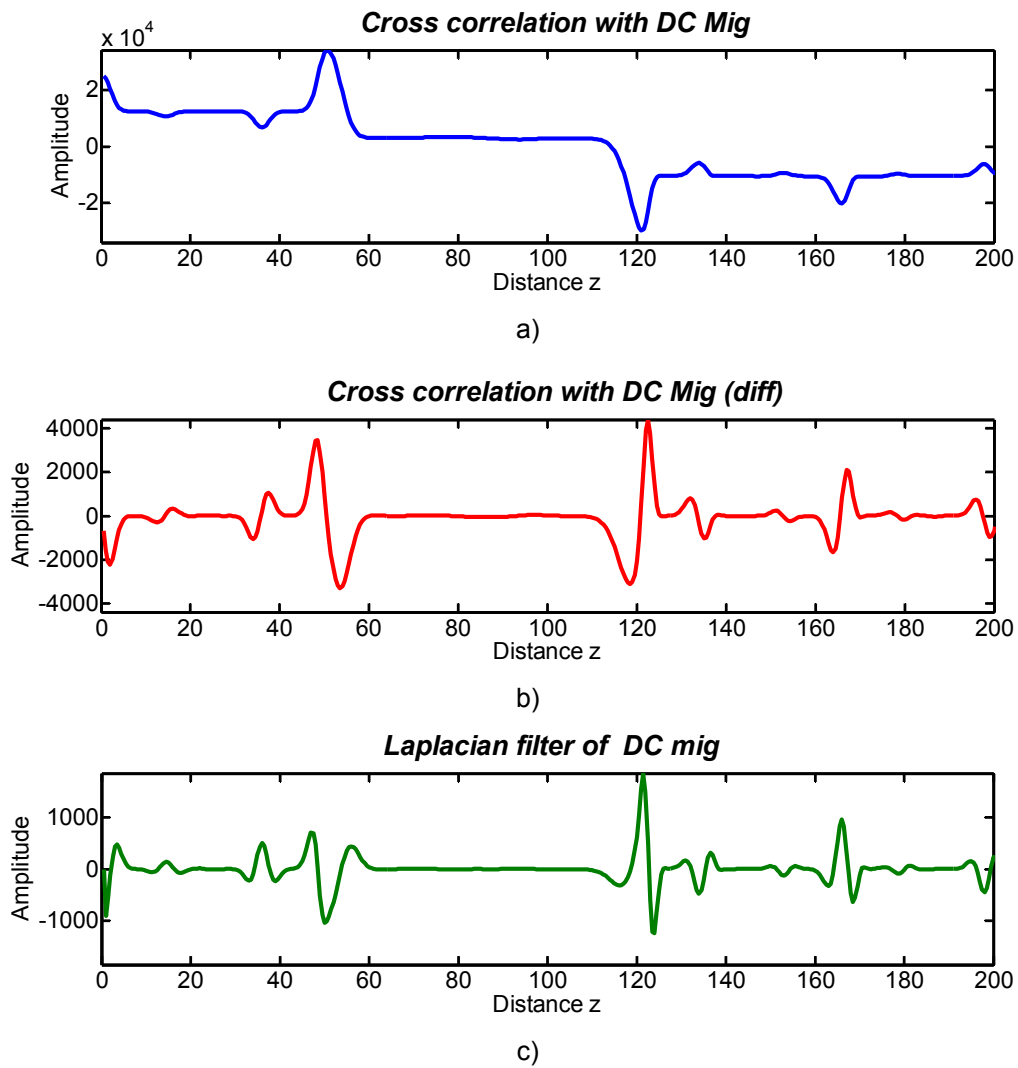

FIG. 23 CC of FM with the reconstructed reverse time wavefield using only the surface IC, a) the windowed CC, b) the differentiated CC, and c) the Laplacian filtered CC.

The CC of the fully modelled wavefield (FM) with the phase shift one-way wavefield using only the surface IC is displayed in Figure 22a. The differentiated CC is in (b), and the Laplacian filtered CC is displayed in (c).
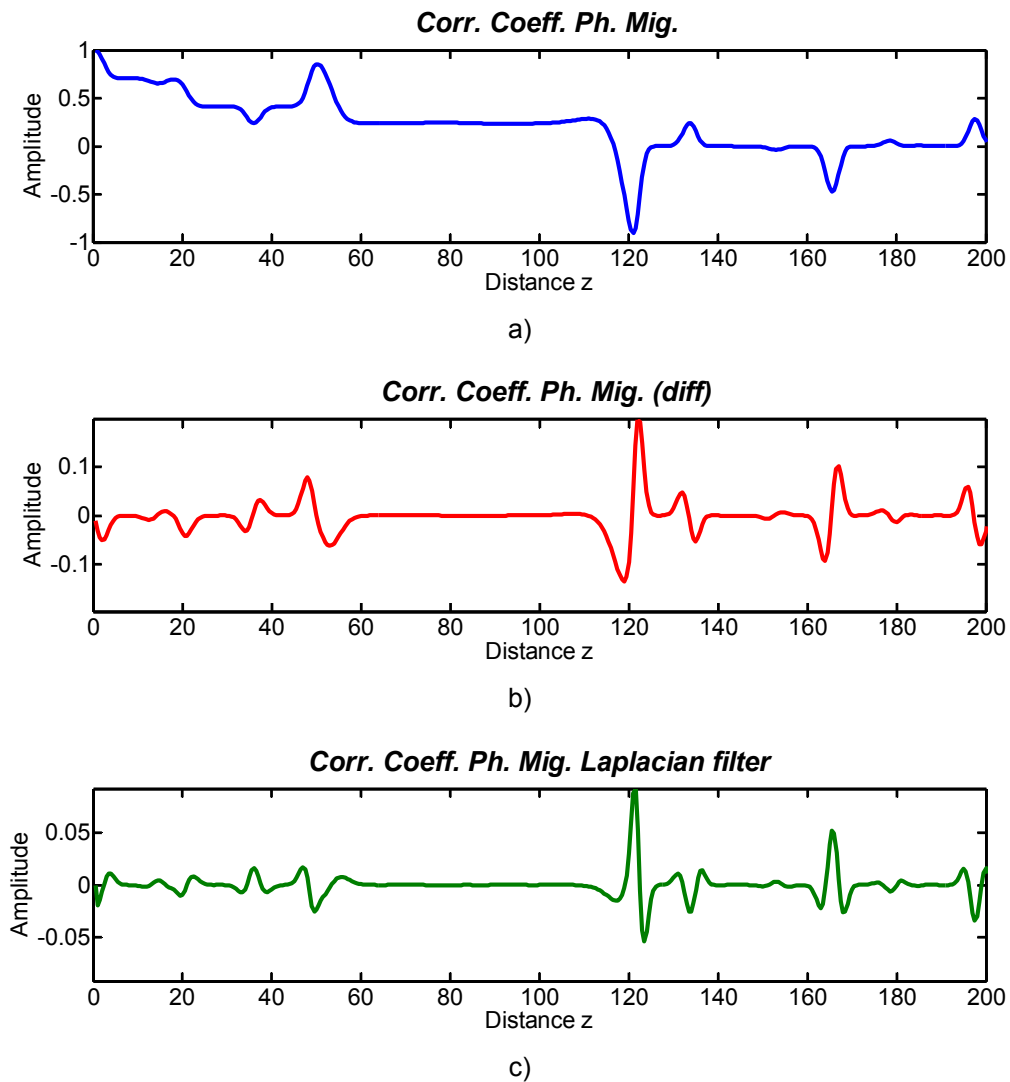

a)

b)

c)

FIG. 24 CC of FM with the reconstructed phase shift with only the surface IC, a) the windowed CC, b) differentiated CC, and c) Laplacian filtered CC.

Points to note

1. Multiples create low frequency artifacts.
2. Multiples create high frequency artifacts.
3. Multiples create more multiples that were not on the forward model.
4. Multiples do not reconstruct.
5. It may be better to remove multiple energy.
6. Alternatives to reverse-time migration:
     a. Downward continuation,
     b. Phase-shift, PSPI,
     c. Finite difference.
7. There may be an advantage in windowing the modelled data using the velocity model.
8. The size of the reflectivity was exaggerated to display artifacts
9. Reverse time migration requires the full volume of data (x, z, t) to be created and stored in memory before the cross-correlation process proceeds.
10. The downward continuation processes perform the cross-correlation process at each downward step.
11. Reverse-time migration can produce a zero-lag correlation during each time step of the reverse time process.

CONCLUSIONS

Multiple energy can align over an interval and remain correlated to produce a constant value at depths. This low frequency energy is difficult to remove.

Alternate forms of migration may be preferable to the Reverse time algorithm.

It may be better to remove the multiple energy with conventional seismic processing, and create forward modelled data without the multiples.

The results used a simple 1D model to visualize the motion of wavefield energy to aid in identifying the artifacts present in the cross-correlation imaging condition. Further tests will be required with more complex and higher dimensional data to fully evaluate the best process to recover the reflectivity.

Oneway migration, such as phase shift, reduces the multiple energy created in the reconstructed wavefield.

ACKNOWLEDGEMENTS

REFERENCES

Claerbout, J. F., 1971, Toward a unified theory of reflector mapping, Geophysics, 36, No. 3, 467-481
method, PhD Dissertation, Department of Geoscience, University of Calgary
Gazdag, J., 1978, Wave equation migration with the phase shift method, Geophysics, Vol. 43, 1342 – 1351.

Liu, H, Zou, Z., and Cui, Y., 2010, Denoising and storage in seismic reverse time migration, Chinese Journal of Geophysics, Vol. 53, N0. 5, 828 - 837

Margrave, G F., K. Innanen, and M. Yedlin, 2012, A Perspective on FullWaveform Inversion, CREWES Research Report, Vol. 24.

Margrave, G F., M. Yedlin, and K. Innanen, 2011, Full waveform inversion and the inverse Hessian, CREWES Research Report, Vol. 23.

Margrave, G F., R. Ferguson, and C. M. Hogan, 2010, Full waveform inversion with wave equation migration and well control, CREWES Research Report, Vol. 22.

Whitmore, N. D. (1983). Iterative Depth Migration by Backward Time Propagation. *1983 SEG Annual Meetin*g, September 11 - 15, Las Vegas, Nevada.

Zaiming Jiang, 2012, Elastic wave modelling and reverse time migration by staggered grid finite difference

APPENDIX

The following table identified the runtimes and memory requirements when using a desktop computer with 8 G of memory. The intent is to demonstrate that processing with very small sample intervals can become impractical with full waveform modelling.

Table 1 Results of varying the sampling size of the data on runtimes and memory requirements.

Nx	Nz	δz m	δt ms	Mem. GB.	Time s
101	401	2.0	1.0	?	Died
201	801	1.0	0.5	?	5.5
401	1601	0.5	0.25	?	5.4
801	3201	0.25	0.125	1.93	6.3 22.9
1601	6201	0.125	0.0625	2.29	7.6 85.4
3201	12801	0.0625	0.03125	3.67	16.5
6401	25601	0.03125	0.015625	7.5+Paging	65.5 14579.7
12801	51201	0.015625	0.0078125		∞